# Physical Simulation Experiments of Momentum Transport Associated with Advecting Vortical Motions

**J. R. Elsnab[1] and J. C. Klewicki[1,2]**

[1]Department of Mechanical Engineering
University of Melbourne, Parkville, Victoria 3010, Australia

[2]Department of Mechanical Engineering
University of New Hampshire, Durham, New Hampshire 03824, USA

## Abstract

We report on experiments investigating velocity-vorticity interactions that underlie the mechanisms of turbulent inertia associated with advecting regions of concentrated vorticity. To isolate mechanisms and expose the full scope of possible interactions, unsteady laminar flow experiments are conducted. These experiments mimic instantaneous flow field interactions known to exist in turbulent wall-flows. Experiments are conducted in a large water tank that involved perturbing laminar vortex rings by altering the natural advection velocity of the ring. Purely advective perturbations to the ring result in a momentary amplification of the Reynolds stress that subsequently decreases back to the unperturbed magnitude. Perturbations below an observed threshold, however, do not cause any changes to the momentum transport characteristics of the vortex ring.

## Introduction

Vortex rings have fascinated researchers for nearly 150 years and can be considered the simplest form of more general concentrated vortices, e.g., cyclones and tornados [1, 12]. Specifically, confined vortex rings exist in the heart when blood exits the left atrium into the left ventricle cavity, and are used as a propulsion mechanism for jellyfish and squid [7, 14]. Numerous researchers have investigated vortex rings and several review articles summarize their behaviour [13, 16]. Their interaction with an angled wall and a normal wall has been investigated by [3, 11]. They have also been interacted with shear layers [2, 12].

One motivation behind investigating vortex rings interacting with surfaces and other flows stems from observed similarities to the coherent motions in boundary layer flows. It is thought that by understanding vortex ring interactions, insight can be gained in respect to wall-bounded turbulent flows. The objective of this study is to investigate the effect of inducing an advection velocity to a vortex ring.

## Methods and Procedures

### Experimental Facility

Vortex rings are generated using a 125 mm piston-cylinder device and a 34.8 mm seamless stainless steel tube that is 800 mm long. The cylinder and SS tube are connected using flexible 38.1 mm tubing. The piston-cylinder motion is precisely controlled using LabView and a stepper motor. A vortex ring is produced at the exit of the tube by converting rotational motion from the stepper motor to translation using a 12.7 mm threaded rod with pitch of 2.11 mm/rev. The outer contour at the exit plane of the
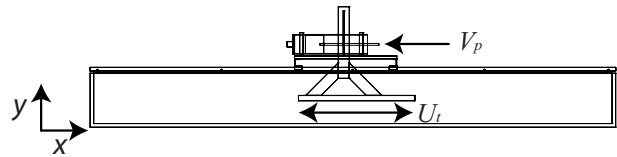


Figure 1: Experimental facility used for the experiments. Note that the stepper motor, timing belt, and flexible tubing are not shown.

tube is machined to form a wedge with tip angle of 10° and length of 6 mm. The vortex ring apparatus (VRA) is allowed to translate on 25.4 mm diameter rails. Translational velocity and displacement of the VRA are controlled using a LabView and an additional stepper motor, which drives a timing belt system that is attached to the VRA. Trapezoidal velocity versus time profiles are implemented in LabView with an impulse configuration, i.e., acceleration time is much less than the overall time interval, $T$. Due to unequal time intervals for the vortex ring generation and translation, the timing is set so that the end of the constant velocity region of each respective velocity curve coincide. Experiments are conducted in a large water tank with width of 1.08 m, length of 3.6 m and height of 0.37 m. A schematic of the apparatus is presented in figure 1.

Vortex rings are formed using a stroke length, $L/D$ of 1.96, where $L$ is the fluid displacement in the tube and $D$ is the SS tube diameter, at a Reynolds number based upon average slug velocity, $\overline{V_s} = 1/T \int v_s(t)dt$ and tube diameter of 2800. Gharib et al. [7] identified the ratio $L/D = \overline{V_s}T/D$ with the formation time. The translation velocity, $U_t$, ranged from $\pm 2.37$ cm/sec, which resulted in a perturbation velocity, $U_t/U_{cl}$, of $\pm 23.9\%$, where $U_{cl}$ is the centerline velocity obtained by spatial averaging in the streamwise direction centred over $0.1D$ along the x-axis ring centerline.

### Experimental Methods

Digital particle imaging velocimetry data are obtained at the wall-normal plane of symmetry (x – y plane). A dual pulse Nd:YAG laser operating at 532 nm is used as the light source. The laser Q-switch timing is synchronized to a CCD camera with resolution $4072 \times 2720$ pixel$^2$ using pulse generators. The water tank is seeded with hollow glass sphere particles, nominally 15 microns in diameter. The time delay between image capture ranges from 2 to 6 ms so that the bulk displacement ranges from 8 to 10 pixels. Image pairs are captured at a rate of 2 Hz. Timing between image acquisition, vortex ring generation, and apparatus translation is accomplished using the output signal from the pulse generator to trigger LabView. Since this timing

method is software based, the accuracy is limited to 0.001 s.

## Data Reduction

A multi-pass, multi-grid, cross-correlation method is utilized to determine the particle displacements with a base interrogation window size of $32 \times 32$ pixel$^2$, which is subsequently divided into four $16 \times 16$ pixel$^2$ windows. A window shift of 8 pixels (50% overlap) is also utilized in the second pass. The particle diameters ranged from 2 to 3 pixels, which results in an RMS uncertainty of $3.7 - 4.3 \times 10^{-4}$ cm [15]. The field of view is $6.6D \times 4.22D$ and starts $2.5D$ from the stopping point of the tube exit. Velocity vector resolution is $0.0141D$ for both the streamwise and wall-normal directions and the uncertainty in velocity is less 1% after averaging the instantaneous vector fields over 35 trials. The kinematic Reynolds stress, $UV$, is obtained by taking the product of the steamwise velocity, $U$ with the wall-normal component, $V$. The spanwise vorticity, $\omega_z$, is obtained by differentiating the velocity field using a least-squares method [6]. The circulation, $\zeta$, on the upper and lower half of the ring is obtained by Stokes theorem, $\equiv \oint_c u \cdot \mathbf{d}l = \int_A \omega_z \mathbf{d}A$, using a two-dimensional version of the trapezoidal rule. The gradient of the Reynolds stress is related to the velocity-vorticity and streamwise gradient of kinetic energy by the following exact relationship

$$\frac{\partial \overline{UV}}{\partial y} + \frac{\partial \overline{UW}}{\partial z} = \overline{\omega_y W} - \overline{\omega_z V} + \frac{1}{2}\frac{\partial}{\partial x}\left(\overline{V^2 + W^2 - U^2}\right), \quad (1)$$

where $W$ is the spanwise velocity and $\omega_y$ is the wall-normal vorticity [8]. Within the wall-normal plane of symmetry, $W$ and $\partial()/\partial z$ are equal to zero. The first two terms on the RHS of equation 1 may be thought of as the rotational component of the motion, and the last term as the irrotational component of the motion [17]. By understanding how the gradient of the Reynolds stress arises, it is thought that the ways in which velocity and vorticity fields interact to generate the apparent inertial force attributable to turbulent eddies.

## Results

A typical $\overline{UV}$ contour plot is shown in figure 2 along with vectors of $U$ and $V$, where $\overline{()}$ represents an average over all of the vector fields. This average is obtained by spatially shifting the vortex ring at each $x/D$ to a fixed streamwise location and then averaging over the instantaneous fields. The magnitude of the spatial shift is based upon the location where the average of the streamwise velocity in the wall-normal direction is maximized. Even though the streamwise evolution of the ring changes, this effect is less than 8% in $U_{cl}$ for cases investigated, therefore, the ensemble averaged results can be considered 'steady'. Since there are four poles in a quadrant configuration in figure 2, a majority of the results presented herein are based upon this spatial quadrant configuration. Integrating each quadrant allows for a comparison to made based upon both a local, i.e., individual quadrant, and a global basis, i.e., summation of the individual quadrants. Specifically, $\overline{UV}/V_s^2$ as a function of $U_t/U_{cl}$, shown in figure 3 depicts a momentary amplification of the Reynolds stress that subsequently decreases back to the unperturbed magnitude. This normalization is based upon a formation parameter. Perturbations below 10%, however, do not cause
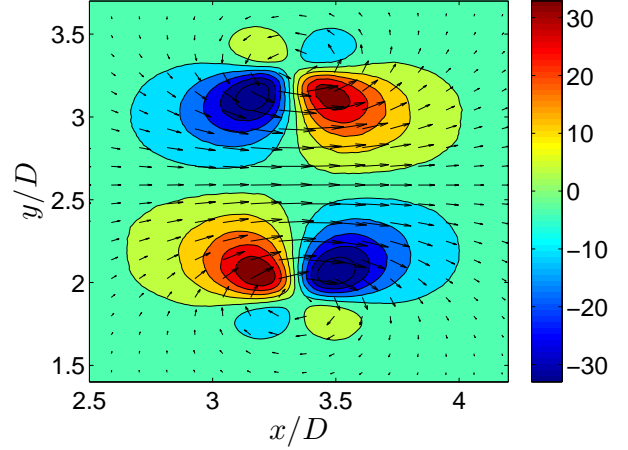


Figure 2: Contours of $\overline{UV}$ [cm$^2$/s$^2$] for $U_t/U_{cl} = 0$ along with velocity magnitude vectors of $U$ and $V$ [cm/s].
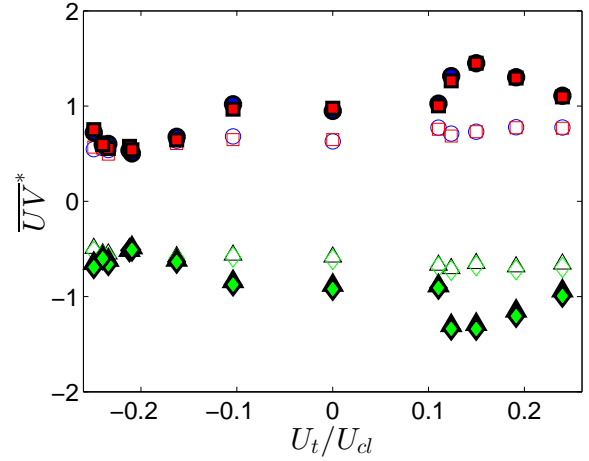


Figure 3: Dimensionless Reynolds stress as a function of the perturbation. Description: Quadrant 1, $\circ$; Quadrant 2, $\triangle$; Quadrant 3, $\square$; and Quadrant 4, $\diamond$. Filled symbols are normalized using $\overline{V_s^2}$ and open symbols, $U_{cl}^2$, respectively.

any changes to the momentum transport characteristics of the vortex ring. However, if the Reynolds stress is normalized by $U_{cl}^2$, a local normalization, the magnitude of $\overline{UV}$ becomes a constant. The average value for the four quadrants from one to four is $-2.24$, $2.20$, $-2.30$, $2.38$ with standard deviation of $0.141$, $0.142$, $0.152$, $0.166$, respectively. Interestingly, for negative perturbations, the maximum deviation in Reynolds stress approaches the average value obtained using a local normalization. The maximum percent difference in $\overline{UV}$ between a zero and positive/negative perturbations of 15% and 21% is 46% and 45%, respectively.

The circulation values presented in figure 4 are based upon the upper and lower half of the ring. The values are normalized using the formation circulation assuming a slug model, which is given as $\overline{V_s}L$, and a local value of $U_{cl}R$, where $R$ is the half distance between the minimum and maximum spanwise vorticity. A slug model is used instead of the boundary layer approximation result,
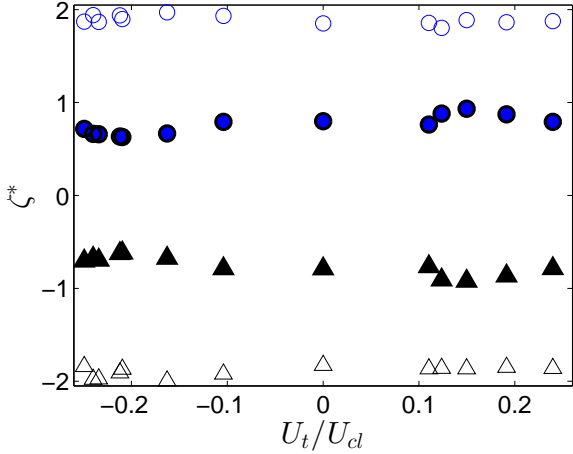
Figure 4: Dimensionless circulation as a function of the perturbation. Description: Quadrant 1 + 2, ○; Quadrant 3 + 4, △. Filled symbols are normalized using $\overline{V_s}L$ and open symbols, $U_{cl}R$.

$\zeta = \overline{V_s}T/2$, presented by Diden [4] since $T < 1$ second for the current experiments. Both normalizations follow the same trend that is exhibited in figure 3, albeit, the formation normalization is not as distinct. The difference between the upper and lower ring circulation is less than 2%.

The nonzero terms on the RHS of equation 1 as function of the applied perturbation are shown in figure 5A and B. The formation normalization is $\overline{V_s^2}/D/2$ and the local normalization is $U_{cl}^2/R$. The data normalized with the formation and local parameters follow the same trend as the Reynolds stress, but both normalizations show more scatter in comparison to figure 3. A global balance of the terms in equation 1 is nominally zero. The mean value for the local normalization is $-0.028 \pm 0.026$ and for the formation normalization, $-0.029 \pm 0.026$. The remainder is attributed to a slight nonzero spanwise velocity.

If $\partial \overline{UV}/\partial y$ is estimated from equation 1 instead of calculated directly, the percent difference is low by approximately $10 - 15\%$. It is not clear at this time why the deviation exists. In well-developed boundary layers, the irrotational part is, on average, about three orders of magnitude smaller than the rotational term [9]; however, for the current investigation, the irrotational term is $1.5\times$ the rotational.

In the context of concentrated regions of vorticity, a critical question relates to whether the local velocity field (momentum field per unit mass) is experiencing a net drag or impulse owing to its interaction with the vorticity field [10]. For idealized vortices these interactions are precisely described in terms of a "drift velocity" between the vortex and the surrounding velocity field [5]. This effect produces a Magnus-type force that can be positive or negative depending on the details of the interaction. The drift velocity is given as

$$\Delta u_i = \epsilon_{ijk}\omega_j \frac{g_k}{\omega_l \omega_l}, \qquad (2)$$

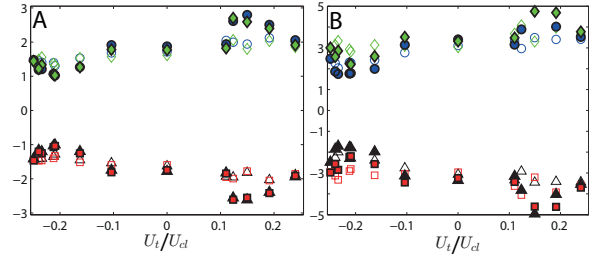where $g_k$ is the nonpotential viscous force given as



Figure 5: Dimensionless rotational term, $\overline{\omega_z V}$, is shown in figure A and the irrotational term, $0.5\partial\left(\overline{V^2} - \overline{U^2}\right)/\partial x$, is shown in figure B as a function of the perturbation. Description: Quadrant 1, ○; Quadrant 2, △; Quadrant 3, □; and Quadrant 4, ◇. Filled symbols are normalized using $\overline{V_s^2}/D/2$ and open symbols, $U_{cl}^2/R$.
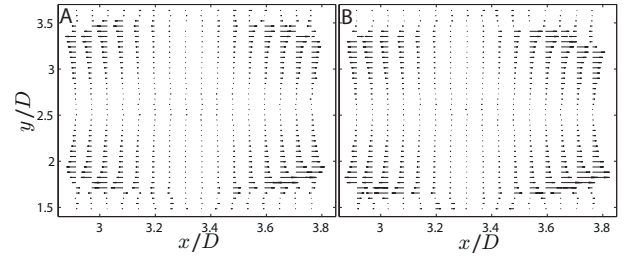


Figure 6: Streamwise drift velocity vectors for figure A ($U_t/U_{cl} = 0$) and figure B ($U_t/U_{cl} = -21.2\%$) in mm/s.

$-v\epsilon_{klm}\partial/\partial x_l \omega_m$ and $v$ is the kinematic viscosity [5]. Equation 2 simplifies to the following components: $\Delta u_x = -v/\omega_z \partial\omega_z/\partial x$ and $\Delta u_y = -v/\omega_z \partial\omega_z/\partial y$. Since the vortex ring is traveling in the streamwise direction, it is expected that there will be a natural asymmetry in $\Delta u_x$. This is qualitatively evident in figure 6, which compares $U_t/U_{cl} = 0$ and $-21.2\%$. Quantitatively, the skewness, $\gamma$, is an indicator of asymmetry and is shown as a function of $U_t/U_{cl}$. For negative perturbations, the skewness increases and subsequently nearly decreases back to zero perturbation. The opposite trend exists for positive perturbations. Both trends are consistent with the $\overline{UV}$ trend. These trends are indicative that the perturbed vortex motion results in a net (integral sense) augmentation or attenuation of the surrounding momentum field.

The gradient of the Reynolds stress, which is a dynamical term that appears in the time averaged Navier–Stokes equations, i.e., 'turbulent force', and acts as a net source or sink of momentum depending upon whether $y < y_m$ or $y > y_m$, where $y_m$ is the position where the Reynolds stress is maximized [10]. Clearly contours of $\partial \overline{UV}/\partial y$ shown in figure 8 are substantially modified by the perturbation, both in magnitude and spatial distribution. For case C, the peak 'force' that the ring is subjected to is highly concentrated, whereas for case A, the 'force' is distributed over a larger area of the ring. For a negative perturbation, $\partial \overline{UV}/\partial y$ is biased towards quadrants 1 and 4, whereas for a positive perturbation, $\partial \overline{UV}/\partial y$ is biased towards quadrants 2 and 3. The trends exhibited in the drift velocity are attributed to the aforementioned biases in $\partial \overline{UV}/\partial y$.
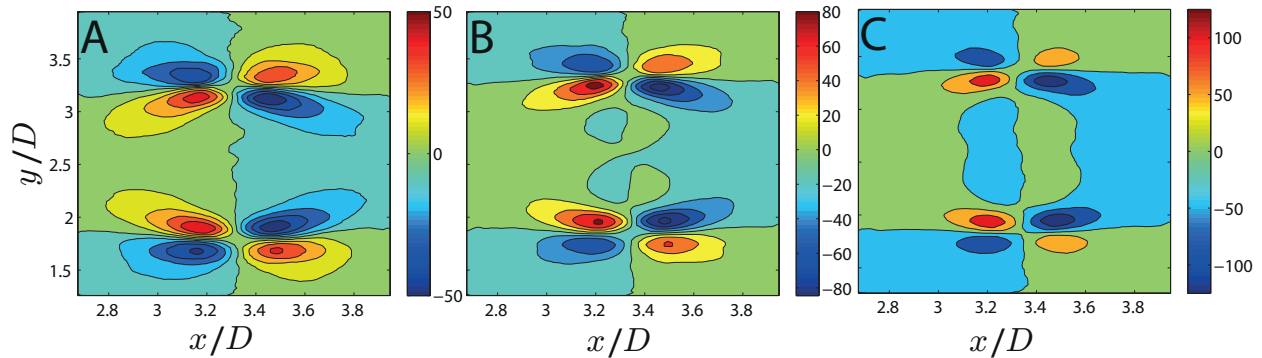
Figure 8: Contours of the wall-normal gradient of the Reynolds stress, [cm/s$^2$], for $U_t/U_{cl}$: figure A = −21.2%, figure B = 0%, and figure C = 15%.



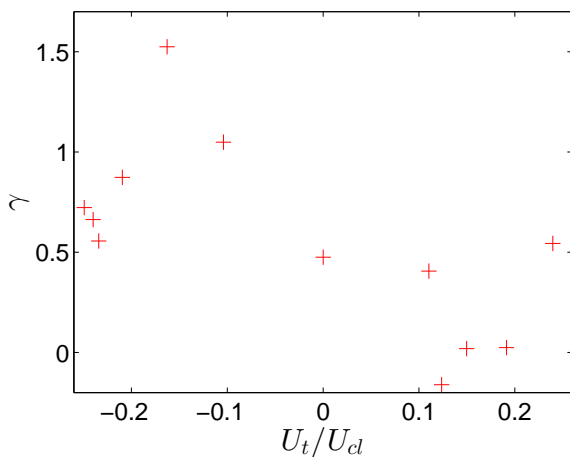Figure 7: Skewness in $\Delta u_x$ as a function of the perturbation.

## Conclusions

An experimental investigation of vortex rings subjected to an induced advection velocity is reported herein. Purely advective perturbations to the ring result in a momentary amplification of the Reynolds stress that subsequently decreases back to the unperturbed magnitude. Perturbations below an observed threshold, however, do not cause any changes to the momentum transport characteristics of the vortex ring. The drift velocity asymmetry is consistent with the notion that the perturbed vortex motion results in a net (integral sense) augmentation or attenuation of the surrounding momentum field.

## Acknowledgements

## References

[1] Akhmetov, D., *Vortex Rings*, Springer, 2009.

[2] Chu, C. and Falco, R., Vortex ring/viscous wall layer interaction model of the turbulence production process near walls, *Exps. Fluids*, **6**, 1988, 305 – 315.

[3] Couch, L. D. and Krueger, P. S., Experimental investi-gation of vortex rings impinging on inclined surfaces, *Exps. Fluids*, **51**, 2011, 1123–1138.

[4] Didden, N., On the formation of vortex rings rolling-up and production of circulation, *J. Applied Math. Phys. (*ZAMP*)*, **30**, 1979, 101–116.

[5] Eyink, G., Turbulent flow in pipes and channels as cross-stream "inverse cascades" of vorticity, *Phys. Fluids*, **20**, 2008, 125101–1–13.

[6] Foucaut, J. and Stanislas, M., Some considerations of the accuracy and frequency response of some deriva-tive filters applied to particle image velocimetry vec-tor fields, *Meas. and Science Tech.*, **13**, 2002, 1058–1071.

[7] Gharib, M., Rambod, E. and Shariff, K., A universal time scale for vortex ring formation, *J. Fluid Mech.*, **360**, 1998, 121–140.

[8] Hinze, J., *Turbulence*, McGraw-Hill, 1975, 2nd edition.

[9] Klewicki, J., Velocity-vorticity correlations related to the gradients of the Reynolds stress in parallel turbu-lent wall flows, *Phys. Fluids A*, **1**, 1989, 1285–1288.

[10] Klewicki, J., Fife, P., Wei, T. and McMurtry, P., A phys-ical model of the turbulent boundary layer consonant with mean momentum balance structure, *Phil. Trans. R Soc. A*, **365**, 2007, 823 – 839.

[11] Lim, T., An experimental study of a vortex ring in-teracting with an inclined wall, *Exps. Fluids*, **7**, 1989, 453–463.

[12] Lim, T., Lua, K. and Thet, K., Does Kutta lift exist on a vortex ring in a uniform cross flow, *Phys. Fluids*, **20**, 2008, 051701–1–4.

[13] Lim, T. and Nickels, T., *Vortex Rings in Fluid Vortices*, Kluwer, Dordrecht, 1995.

[14] Linden, P. and Turner, J., Vortex rings and aquatic propulsion, *Proc. R. Soc. Lond. B*, **271**, 2004, 647–653.

[15] Raffel, M., Willert, C. and Kompenhans, J., *Particle image velocimetry: a practical guide*, Springer, Berlin, 1998.

[16] Shariff, K. and Lenard, A., Vortex rings, *Annual Re-view of Fluid Mechanics*, **24**, 1992, 235–279.

[17] Townsend, A., Equilibrium layers and wall turbu-lence, *J. Fluid Mech.*, **11**, 1961, 97–120.